# Ab Initio and RRKM Study of the Reaction of ClO with HOCO Radicals

**Hua-Gen Yu**[†] **and Joseph S. Francisco***[,‡]

*Department of Chemistry, Brookhaven National Laboratory, Upton, New York 11973 and Department of Chemistry, Purdue University, West Lafayette, Indiana 47907*

*Received: April 30, 2009; Revised Manuscript Received: September 23, 2009*

The reaction pathways for the ClO + HOCO reaction have been explored using the coupled-cluster method to locate and optimize the critical points on the ground-state potential-energy surface. Results show that the ClO + HOCO reaction can produce Cl + HOC(O)O, HOCl + $CO_2$, HCl + $CO_3$, and HClO + $CO_2$ via an addition or a direct hydrogen abstraction reaction mechanism. The reaction kinetics has been studied using the variational RRKM theory. It is found that the ClO + HOCO reaction is fast and has a negative temperature dependence at low temperatures. At room temperature, the thermal rate coefficient is obtained as $4.26 \times 10^{-12}$ cm$^3$ molecules$^{-1}$ s$^{-1}$ with product branching fractions of Cl (0.518), HOCl (0.469), HCl (0.01), and HClO (0.003) at zero pressure. The Cl + HOC(O)O products are major, compared to the HOCl + $CO_2$ products, because of the loose transition state along the dissociation pathway to eliminate Cl. In addition, the RRKM/master equation simulations indicate that the stabilization of the HOC(O)OCl intermediates is noticeable at moderate pressures as its thermal rate constants reach about $6.0 \times 10^{-13}$ cm$^3$ molecules$^{-1}$ s$^{-1}$. In contrast, the other product branching ratios for the ClO + HOCO reaction are weakly dependent on pressure.

## I.. Introduction

The HOCO radical is a key intermediate that plays an important role in the oxidation of CO to $CO_2$ involving OH radicals[1−6] via

$$\begin{array}{c} \mathrm{OH + CO \rightarrow HOCO^* \rightarrow H + CO_2} \\ \downarrow\uparrow \mathrm{M} \\ \mathrm{HOCO} \end{array}$$

DeMore[7] and others[8−10] have shown that the HOCO radical is stable and has noticeable abundance in atmospheric and combustion environments. It has two conformers:[11,12] *cis*-HOCO and *trans*-HOCO, while the stable *trans*-HOCO has been observed by a few groups[13−19] using millimeter-wave, infrared magnetic resonance (FIR-LMR), and infrared action spectroscopic techniques. There are a few experimental studies that focus on the reactions of HOCO with other radicals. Moore et al.[20] and Smith et al.[21] measured the thermal rate coefficients for the $O_2$ + HOCO reaction. The reaction rate constant ($2.1 \times 10^{-12}$ cm$^3$ molecules$^{-1}$ s$^{-1}$) is only moderate due to a small classical barrier of 0.7 kcal/mol in the entrance channel.[22] Another reaction is the Cl + HOCO reaction.[23] Experimental results show that the reaction is quite fast and produces only the products HCl + $CO_2$ at room temperature. Recently, molecular dynamics calculations[24] predict a thermal rate constant of $3.0 \times 10^{-11}$ cm$^3$ molecules$^{-1}$ s$^{-1}$ (298 K) for the Cl + HOCO → HCl + $CO_2$ reaction, which is consistent with the experimental results of Li et al.[23]

In addition to the experimental studies of the reactions of HOCO, there are several theoretical dynamics and/or kinetics investigations on the reactions of the HOCO radical with other small radicals[22,24−30] such as H, Cl, O, $O_2$, NO, OH, $HO_2$, and $CH_3$. For more details, the reader can refer to the recent comprehensive review on HOCO radical chemistry.[31] In general, the HOCO radical acts as a donor of hydrogen to the reaction partners. Here, it is worth mentioning the reaction of OH radicals with HOCO, which, at room temperature, has a calculated thermal rate coefficient[27] of $1.0 \times 10^{-11}$ cm$^3$ molecules$^{-1}$ s$^{-1}$ that is nearly 2 orders of magnitude larger than that of the OH + CO reaction. Therefore, the OH + HOCO reaction has important ramifications for the removal of HOCO radicals in both atmospheric and combustion processes[32] and has apparent implications for the lifetime of the HOCO radical from laboratory studies. In other words, the two-step reaction mechanism, (a) OH + CO → HOCO and (b) OH + HOCO → $H_2O$ + $CO_2$, becomes competitive with the one-step OH + CO → H + $CO_2$ reaction for the oxidation of CO to $CO_2$ involving OH radicals.

Chlorine oxide, ClO, is an important chlorine species in atmospheric chemistry. The study of the reaction of ClO with HOCO is interesting, but in fact, little is known about this reaction. If using the general hydrogen abstraction mechanism mentioned above, one can expect that HOCl and $CO_2$ would be the major products in the ClO + HOCO reaction, similar to the ClO + $HO_2$ reaction[33−40] and the OH + HOCO reaction.[27] In this work, the ClO + HOCO reaction is investigated using high-level ab initio quantum chemistry methods and kinetics approaches. The essential critical points on the potential-energy surface are examined to understand the details of the reaction mechanism. Variational RRKM (Rice−Ramsperger−Kassel−Marcus) theory is used to investigate the kinetics of the reaction, where the thermal rate coefficients and product branching ratios are determined.

## II. Computational Method

The potential-energy surface for the ClO + HOCO reaction is explored with two levels of theory. The first one is the quadratic configuration interaction with single- and double-excitation method (QCISD)[41] with the Dunning correlation-

* To whom correspondence should be addressed. E-mail: francisc@purdue.edu.
† Brookhaven National Laboratory.
‡ Purdue University.

10.1021/jp9040088 CCC: $40.75 
Published on Web 10/15/2009

consistent cc-pVDZ basis set.[42,43] It is used in preliminary searches of global minima and transition states. Full geometry optimizations are performed for all structures using Schlegel's method[44] with tolerances to better than 0.001 Å for bond lengths and 0.01° for angles, with a self-consistent field convergence of at least $10^{-9}$ on the density matrix. The residual rms (root mean square) force is less than $10^{-4}$ au. Vibrational frequency calculations are performed to determine whether the critical points obtained are either minima or transition states on the potential-energy surface, i.e., all positive frequencies (minima) or one imaginary frequency (first-order saddle points). The Hessians from these optimizations are then used to search for the global minima and transition states using the second level of theory, the coupled-cluster method (CCSD(T)) including single and double excitations along with a perturbative correction for the triple excitations.[45,46] The following eigenvalue method is used with the Hessians from QCISD optimizations. Vibrational frequency calculations are repeated to confirm the critical points reoptimized at the CCSD(T)/cc-pVDZ level of theory. To improve the energetics, optimizations are carried out with the CCSD(T) method using the larger cc-pVTZ basis set. In addition, a single-point energy calculation is performed at the CCSD(T)/cc-pVTZ geometries using the CCSD(T)/cc-pVQZ method. As spin contamination may produce inaccurate total energies when performing these calculations, the total spin value $\langle S^2 \rangle$ is closely monitored. The largest preannihilation deviation from the expected $\langle S^2 \rangle$ value of 0.75 for open-shell species is less than 3%, and therefore, spin contamination is considered negligible for the reaction system.

The kinetics of the reaction is investigated using a RRKM approach. The bimolecular rate coefficients of the ClO + HOCO reaction are approximately calculated by the variational RRKM theory as[47−49]

$$k_j(T) = g_e \frac{\delta_r}{h} \frac{Q_{tr}^{\ddagger}(T)}{Q_{ClO}(T) Q_{HOCO}(T)} \sum_{J=0}^{\infty} (2J+1) \int N^{\ddagger}(E, J; s_j) e^{-E/k_B T} \, dE \quad (1)$$

where the sum of states of the transition state for a given total angular momentum $J$ at energy $E$ is computed by integrating the tunneling corrected density of states ($\rho^{\ddagger}(E,J)$) as

$$N^{\ddagger}(E, J; s_j) = \sum_{K=-J}^{J} \int_{-V_{a0}^G}^{E-V_{a0}^G} \kappa_j(\varepsilon) \rho^{\ddagger}[E - V_a^G(s_j) - E_{rot}^{\ddagger}(J, K; s_j), J] \, d\varepsilon \quad (2)$$

with the rotational energy of the transition state

$$E_{rot}^{\ddagger}(J, K; s_j) = \frac{1}{2}(B + C) J(J+1) + \left[A - \frac{1}{2}(B + C)\right] K^2 \quad (3)$$

and $A$, $B$, and $C$ are rotational constants. $\kappa_j(\varepsilon)$ is the tunneling correction factor, which is evaluated using the Eckart barrier model.[50] The barrier height and curvature are determined from the one-dimensional vibrationally adiabatic ground-state potential curve

$$V_a^G(s_j) = V_{MEP}(s_j) + \frac{1}{2} \sum_{i=1}^{3N-7} h\nu_i(s_j) \quad (4)$$

for the $j$th pathway at the maximum point. Here, $V_{MEP}(s_j)$ is the potential along the minimum energy path $s_j$ and $\nu_i(s_j)$ are the projected frequencies orthogonal to the reaction path. Furthermore, $g_e$ and $\delta_r$ are the electronic statistical factor and the number of degenerate reaction paths for the $j$th bimolecular reaction pathway, respectively. The superscript "‡" refers to the variational transition state that minimizes the rate coefficient $k_j(T)$ along the reaction path. $Q_x(T)$ are the partition functions per unit volume of the reactants and transition state. They are calculated in the usual manner. The subscript "tr" denotes only the translational component of partition functions.

The microcanonical RRKM reaction rate constant of a unimolecular reaction to the product channel $p$ is given by[51−53]

$$k_p(E^*) = \frac{\sigma_p (I_a^{\ddagger} I_b^{\ddagger} I_c^{\ddagger})^{1/2} N_v(E^{\ddagger})}{h \rho_{\Sigma}(E^*)} \quad (5)$$

Here, $\sigma_p$ is the number of degenerate reaction paths obtained from all isomers. $I_a^{\ddagger}$ are the moment of inertia of the (variational) transition state. By using its vibrational density of states $\rho_v(E)$ and the corresponding Eckart tunneling transmission coefficient ($\kappa_v(\varepsilon)$), the sum of states is computed by

$$N_v(E^{\ddagger}) = \int_{-E_0}^{E-E_0} \kappa_v(\varepsilon) \rho_v(E^{\ddagger} - E_0 - \varepsilon) \, d\varepsilon \quad (6)$$

$\rho_{\Sigma}(E^*)$ is the density of states of the HOC(O)OCl intermediate. As the intermediate has four stable isomers, the density of states can be written as

$$\rho_{\Sigma}(E) = \sum_{l \in \text{isomers}} (I_a^l I_b^l I_c^l)^{1/2} \rho_v^l(E - E_0^l) \quad (7)$$

where $E_0^l$ is the zero-point energy level of the $l$'s isomer. Since the molecule of interest is heavy, its rotational energy spacings are rather small. In this work, the rovibrational convolution integrals for the sum of states and the density of states have been integrated using an energy shift approach in the rotational degrees of freedom. We also used the fact that the four isomers are separated by very low barriers (~8.0 kcal/mol) according to our ab initio calculations, so that they are nearly free to convert from each other at the collision energies of the ClO + HOCO reaction. In other words, the system is treated as a single-well problem rather than a multiwell one. The averaging factor of four conformers is considered in the parameter $\sigma_p$ in eq 5. For instance, $\sigma_p$ is four for the Cl + HOC(O)O product. After taking the isomerization summation factor in the density of states in eq 7 into account, the final net contribution of the degenerate paths to $k_p(E^*)$ is unity as it should be. In calculations, both the sum of states and the density of states are calculated using the Beyer−Swinehart direct count method.[54]

Furthermore, the lifetime of the HOC(O)OCl intermediate can be written as

$$\tau(E^*) = \frac{1}{\sum_p k_p(E^*)} \quad (8)$$

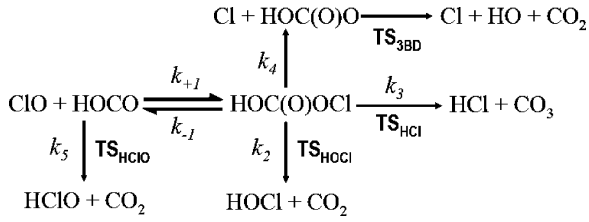


**Figure 1.** Reaction scheme for the ClO + HOCO reaction, where the transition states are also labeled by **TS**s.

where the summation runs over all the dissociation paths of the intermediate. The product branching fractions are determined by

$$f_p(E^*) = k_p(E^*)\tau(E^*) \tag{9}$$

and the thermal average (with respect to the ClO + HOCO reactants) results are given approximately by

$$f_p(T) = \frac{\int \sum_J (2J+1) f_p(E^*) N^{\ddagger}(E,J;s_j) e^{-E/k_B T}\, dE}{\int \sum_J (2J+1) N^{\ddagger}(E,J;s_j) e^{-E/k_B T}\, dE} \tag{10}$$

Since the thermal average is performed for the bimolecular reaction, the energy $E$ is relative to the asymptote of ClO + HOCO. However, the fractions $f_p(E^*)$ are evaluated in terms of the HOC(O)OCl intermediates. Therefore, the corresponding energy used should be converted by the relationship $E^* = E + D_0$, where $D_0$ is the bond dissociation energy of the complex into ClO + HOCO. The sum of states $N^{\ddagger}(E,J;s_j)$ is given in eq 2.

All electronic structure calculations on stationary points are carried out using the Gaussian 03 program,[55] while the intrinsic reaction paths are performed with the MolPro program package.[56]

## III. Results and Discussion

**A. Reaction Pathways for the ClO + HOCO Reaction.** There are two major pathways for the ClO + HOCO reaction as shown in Figure 1. One is direct hydrogen abstraction from the HOCO radical by ClO. The second route is through the addition of the ClO radical into HOCO to form a HOC(O)OCl intermediate that can be stabilized or undergo unimolecular decomposition to generate products. A schematic energy diagram including the zero-point energy corrections is also displayed in Figure 2. It is not plotted according to the intrinsic reaction coordinate IRC. On the IRC paths, the **TS$_{HOCl}$** transition state is connected with both (trans,cis) and (cis,trans) conformers whereas **TS$_{HCl}$** links to the (trans,trans) one.

The direct abstraction of hydrogen from HOCO by ClO involves the approach of the incoming atom (either oxygen or chlorine) of ClO along the HO axis to HOCO. If the incoming atom is Cl, the HClO + $CO_2$ products will be produced. The corresponding transition state is denoted as **TS$_{HClO}$** in Figure 3. It is noticed that the barrier height is very sensitive to the basis set size. In this work, we determined that the vibrationally adiabatic ground-state barrier height is 2.7 kcal/mol at the CCSD(T)/cc-pVTZ//CCSD(T)/6-311G(2df,2p) level of theory. On the other hand, if the incoming atom is O, the products are HOCl and $CO_2$. At the QCISD level of theory, we are unable to locate such a direct H abstraction transition state for the HOCl + $CO_2$ products. Because the ClO radical approaching HOCO along the HO axis moves off the axis to add onto the carbon atom in HOCO due to the potential ridge at the Cl−O−HOCO configurations. This finding indicates that the addition reaction of ClO to form HOC(O)OCl intermediate is the preferable route to the direct hydrogen abstraction pathways.

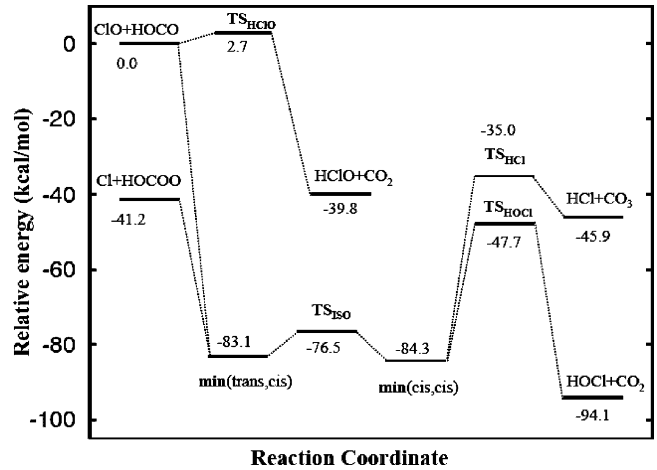


**Figure 2.** Schematic energy diagram for the ClO + HOCO reaction calculated at the CCSD(T)/cc-pVQZ level of theory, where the zero-point energies are taken from the CCSD(T)/cc-pVDZ results. The energy for the **TS$_{HClO}$** transition state is taken from the CCSD(T)/cc-pVTZ//CCSD(T)/6-311G(2df,2p) result.

**B. Formation of the HOC(O)OCl Intermediate.** The HOC(O)OCl intermediate has four conformational structures. They can be classified by the two dihedral angles: $\tau$(HOCO″) and $\tau$(O″CO′Cl). A dihedral angle of 0° (or 180°) refers to cis (or trans). The conformers of HOC(O)OCl are defined in Table 1 and also displayed in Figure 4. All four conformers have been optimized at the CCSD(T)/cc-pVDZ and CCSD(T)/cc-pVTZ levels of theory. Vibrational frequency calculations show all positive frequencies for each species, thus indicating that they are stable minima.

Table 2 shows that the most stable conformer is the (cis,cis) structure. The least stable one has the (trans,trans) conformation. The energy difference between the (cis,cis) and the (trans,trans) structures is only 4.3 kcal/mol at the best level of theory, CCSD(T)/cc-pVQZ//CCSD(T)/cc-pVTZ. In particular, the isomerization barrier is rather low. The barrier height (**TS$_{ISO}$**) from the (cis,cis) conformer to the (trans,cis) one is predicted be 8.8 kcal/mol at the CCSD(T) method. If the zero-point energy corrections are included, the vibrational ground-state adiabatic barrier height becomes 7.8 kcal/mol. The isomerization barriers were also examined using the B3LYP/6-31G(d) DFT method. The energy difference between the (cis,cis) and (trans,trans) conformers is obtained as 3.7 kcal/mol, whereas the **TS$_{ISO}$** barrier height is 8.6 kcal/mol from the (cis,cis) structure. The B3LYP results are in good agreement with the high-level CCSD(T) values, which allow us to estimate the barrier heights among the conformers at the cheaper DFT method. It gives the isomerization barriers as 9.3 kcal/mol from (trans,cis) to (trans,trans), 7.6 kcal/mol from (trans,trans) to (cis,trans), and 8.7 kcal/mol from (cis,cis) to (cis,trans).

**C. Dissociation Pathways for HOC(O)OCl.** The optimized geometries for species involved in the ClO + HOCO reaction are collected in the Supporting Information.[57] The vibrational frequencies and rotational constants of these species are summarized in Table 3, whereas their electronic energies and zero-

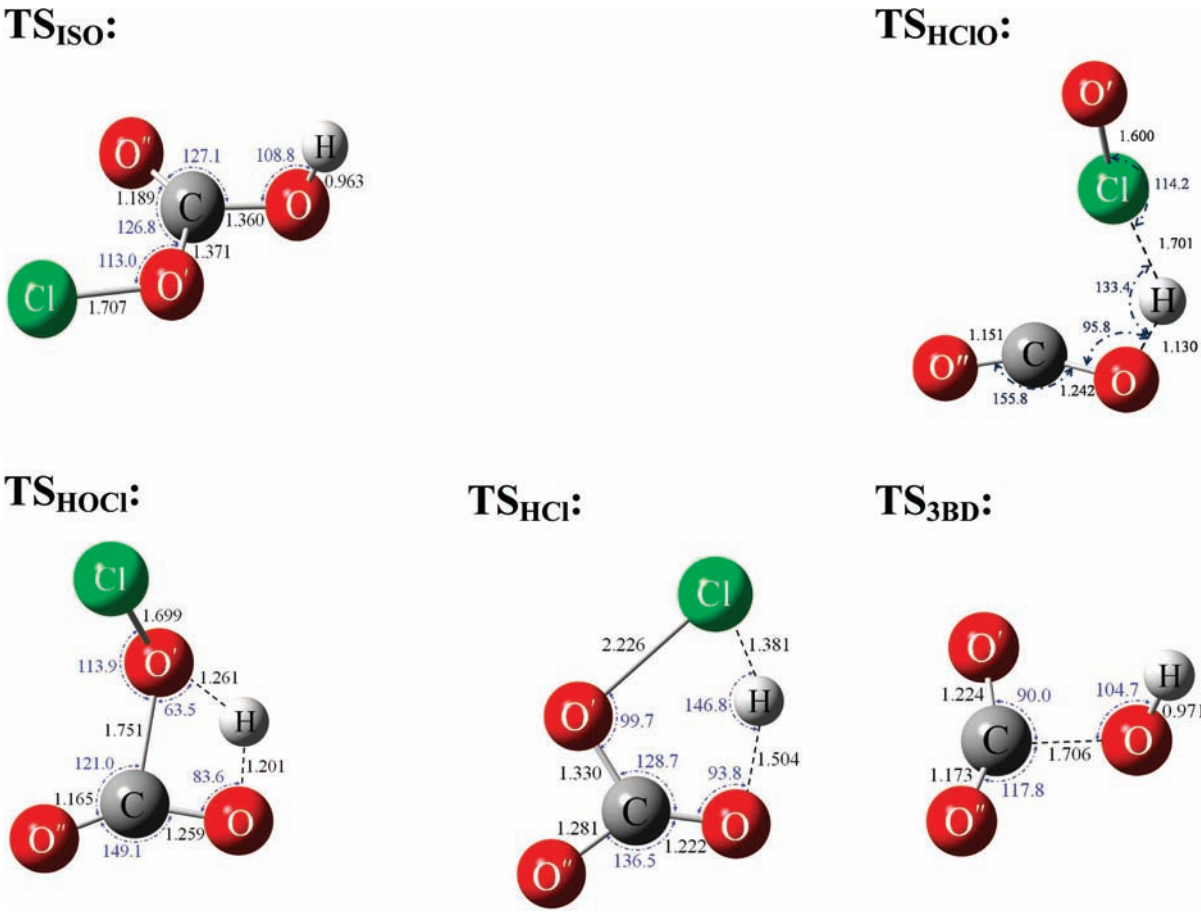


**Figure 3.** Structures for transition states involved in the ClO + HOCO reaction. $\mathbf{TS_{HOCl}}$ is the four-center transition state for HOC(O)OCl → HOCl + $CO_2$. $\mathbf{TS_{HCl}}$ is the five-center transition state for HOC(O)OCl → HCl + $CO_3$. $\mathbf{TS_{HClO}}$ is the direct hydrogen abstraction transition state to HClO + $CO_2$. $\mathbf{TS_{ISO}}$ is the isomerization barrier between (*cis*,*cis*)-HOC(O)OCl and (*trans*,*cis*)-HOC(O)OCl conformers, and $\mathbf{TS_{3BD}}$ is the transition state for the HOCOO → OH + $CO_2$ reaction.

**TABLE 1: CCSD(T) Geometries for the HOC(O)OCl Conformers and the Isomerization Transition State $TS_{ISO}$ between the (cis,cis) and (trans,cis) Conformers (where lengths are Angstroms and angles in degrees)**

| | (cis,cis) | | (cis,trans) | | (trans,cis) | | (trans,trans) | | $TS_{ISO}$ | |
|---|---|---|---|---|---|---|---|---|---|---|
| coordinate | cc-pVDZ | cc-pVTZ | cc-pVDZ | cc-pVTZ | cc-pVDZ | cc-pVTZ | cc-pVDZ | cc-pVTZ | cc-pVDZ | cc-pVTZ |
| O′Cl | 1.741 | 1.700 | 1.758 | 1.712 | 1.739 | 1.700 | 1.768 | 1.715 | 1.750 | 1.707 |
| CO′ | 1.376 | 1.366 | 1.369 | 1.362 | 1.393 | 1.383 | 1.400 | 1.393 | 1.379 | 1.371 |
| CO″ | 1.201 | 1.195 | 1.203 | 1.197 | 1.194 | 1.187 | 1.196 | 1.190 | 1.196 | 1.189 |
| CO | 1.347 | 1.341 | 1.343 | 1.337 | 1.346 | 1.339 | 1.336 | 1.330 | 1.367 | 1.360 |
| OH | 0.972 | 0.965 | 0.972 | 0.966 | 0.972 | 0.965 | 0.972 | 0.967 | 0.967 | 0.963 |
| O″CO′ | 128.0 | 127.6 | 118.7 | 119.0 | 127.4 | 127.0 | 115.9 | 116.6 | 127.2 | 126.8 |
| CO′Cl | 112.3 | 112.4 | 117.3 | 117.5 | 113.2 | 113.1 | 117.2 | 117.3 | 112.9 | 113.0 |
| COH | 104.5 | 105.4 | 104.3 | 105.1 | 107.7 | 108.9 | 109.6 | 110.3 | 107.4 | 109.1 |
| HOCO″ | 0.0 | 0.0 | 0.0 | 0.0 | 180.0 | 180.0 | 180.0 | 180.0 | 92.2 | 92.4 |
| O″CO′Cl | 0.0 | 0.0 | 180.0 | 180.0 | 0.0 | 0.0 | 180.0 | 180.0 | −0.7 | −0.5 |

point energies are listed in Table 4. The equilibrium structures of some important transition states are also displayed in Figure 3.

To check the reliability of the calculations for the energetics, the heat of reaction for the ClO + HOCO → HOCl + $CO_2$ route is examined. The heats of formation of all the species are well known from the literature: HOCl (−16.7 ± 0.6),[58] $CO_2$ (−93.97 ± 0.01),[59] HOCO (−43.9 ± 0.5),[60] and ClO (24.20 ± 0.02)[61] in kcal/mol at 0 K. Using these heats of formation, the heat of reaction obtained is −92.2 ± 1 kcal/mol (0 K). The CCSD(T) methods (see Table 5) predict a heat of reaction of −94 kcal/mol with an error of 1.8 kcal/mol. The results also suggest that the most thermodynamically favorable pathway is the formation of HOCl + $CO_2$.

The well depth for the formation of the HOC(O)OCl (cis,cis) conformation is 84.3 kcal/mol (see Figure 2) relative to the ClO + HOCO reactants at the CCSD(T)/cc-pVQZ//CCSD(T)/cc-pVTZ level of theory. However, with respect to the asymptote of HOCl + $CO_2$, this intermediate is unstable. However, its dissociation has to overcome a noticeable barrier.

There are three major dissociation pathways for the HOC(O)OCl intermediate in addition to such energy-inaccessible dissociation pathways as H + OC(O)OCl and HCO + $ClO_2$. The first is the four-center elimination reaction to produce HOCl + $CO_2$ via the transition state $\mathbf{TS_{HOCl}}$ shown in Figure 3. The $\mathbf{TS_{HOCl}}$ transition state has the following equilibrium geometries: a HOC angle of 83.6°, a OCO′ angle of 89.9°, a C−O′ bond of 1.755 Å, and a O−H bond of 1.201 Å. Compared with the

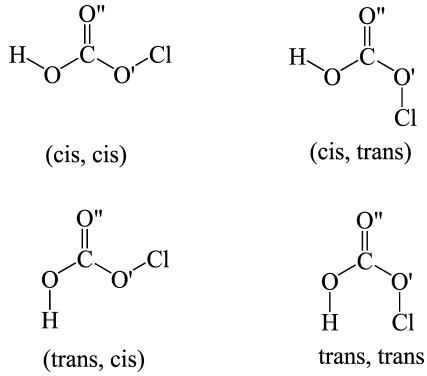


**Figure 4.** Structures of four HOC(O)OCl conformers with their definitions.

corresponding bond lengths in the HOC(O)OCl intermediate, they are longer by 28% for the C−O′ bond and 24% longer for O−H. The structural changes suggest that the HOC(O)OCl → HOCl + $CO_2$ reaction has a late transition state (for the complete structural parameters, see the Supporting Information[57]). The vibrational frequencies of **$TS_{HOCl}$** show that the transition state is a first-order saddle point with an imaginary frequency of 1644*i* $cm^{-1}$. In particular, it has a (trans,cis) configuration of HOC(O)OCl.

Since the global minimum of HOC(O)OCl has the (cis,cis) conformation, in order to access the four-center HOCl + $CO_2$ reaction pathway, the HOC(O)OCl (cis,cis) conformer has to rotate into the (trans,cis) conformation through a small barrier (see **$TS_{ISO}$** in Figure 3) with a barrier height of 7.8 kcal/mol. Nevertheless, the barrier height for the HOC(O)OCl (trans,cis) → HOCl + $CO_2$ dissociation reaction is as high as 35.5 kcal/mol, calculated at the CCSD(T)/cc-pVQZ//CCSD(T)/cc-pVTZ level of theory.

The second dissociation pathway involves breaking the O′−Cl bond to give the products Cl and HOC(O)O. The O′−Cl bond dissociation energy is calculated to be 43.1 kcal/mol from the HOC(O)OCl (cis,cis) conformation at the CCSD(T)/cc-pVQZ//CCSD(T)/cc-pVTZ level of theory. The ClO + HOCO → Cl + HOC(O)O reaction will release a heat of 41.2 kcal/mol. Since the Cl + HOC(O)O asymptote is only 6.5 kcal/mol above the transition state (**$TS_{HOCl}$**), leading to the HOCl + $CO_2$ products, the HOC(O)OCl → HOC(O)O + Cl dissociation could be a competitive reaction with HOC(O)OCl → HOCl + $CO_2$. This is because the former dissociation process does not involve any classical barrier. Interestingly, the product HOC(O)O may have enough energy to further dissociate into OH + $CO_2$. The CCSD(T)/cc-pVQZ//CCSD(T)/cc-pVTZ calculations predict the barrier height to be 18.9 kcal/mol, which is substantially smaller than the reaction exothermicity of 41.2 kcal/mol. Therefore, the resulting HOC(O)O radicals may carry sufficient internal energy to overcome the barrier to produce OH + $CO_2$. Consequently, this secondary decomposition reaction would lead the overall reaction to the three-body dissociation reaction: ClO + HOCO → Cl + OH + $CO_2$.

The third dissociation involves the formation of HCl + $CO_3$ through a five-center transition state **$TS_{HCl}$**, as shown in Figure 3. The H−O and Cl−O′ bonds of **$TS_{HCl}$** (see ref 57) are elongated to 1.504 and 2.226 Å from the equilibrium geometries 0.965 and 1.700 Å of HOC(O)OCl (cis,cis), respectively. Like

**TABLE 2: Energy Analysis for the HOC(O)OCl Conformers and the Isomerization Transition State $TS_{ISO}$**

| | | | CCSD(T) energy/au | | | relative electronic energy/kcal.mol$^{-1}$ | | |
|---|---|---|---|---|---|---|---|---|
| structure | τ(HOCO″) | τ(ClO′CO″) | cc-pVDZ | cc-pVTZ | cc-pVQZ | cc-pVDZ | cc-pVTZ | cc-pVQZ |
| (cis,cis) | 0.0 | 0.0 | −723.36397 | −723.71085 | −723.81816 | 0.0 | 0.0 | 0.0 |
| (cis,trans) | 180.0 | 0.0 | −723.36060 | −723.70738 | −723.81475 | 2.1 | 2.2 | 2.1 |
| (trans,cis) | 0.0 | 180.0 | −723.36185 | −723.70879 | −723.81616 | 1.3 | 1.3 | 1.4 |
| (trans,trans) | 180.0 | 180.0 | −723.35532 | −723.70357 | −723.81122 | 5.4 | 4.6 | 4.3 |
| **$TS_{ISO}$** | 0.0 | 92.2[a], 92.4[b] | −723.34972 | −723.69688 | −723.80419 | 8.9 | 8.8 | 8.8 |

[a] CCSD(T)/aug-cc-pVDZ-optimized results. [b] CCSD(T)/aug-cc-pVTZ-optimized results.

**TABLE 3: Vibrational Frequencies[a] and Rotational Constants[b] for the Species Involved in the ClO + HOCO Reaction (min refers to the minima of HOC(O)OCl)**

| | | rotational constants/GHz | | |
|---|---|---|---|---|
| species | vibrational frequencies/$cm^{-1}$ | *A* | *B* | *C* |
| ClO | 753 | 0 | 18.078 | 18.078 |
| $CO_2$ | 2399, 1338, 650, 650 | 0 | 11.614 | 11.614 |
| $CO_3$ | 2060, 1074, 1018, 670, 568, 538 | 24.017 | 9.320 | 6.715 |
| HCl | 3018 | 0 | 316.190 | 316.190 |
| HClO | 2595, 880, 591 | 337.746 | 17.765 | 16.877 |
| HOCl | 3770, 1240, 675 | 607.801 | 14.875 | 14.520 |
| HOCO | 3820, 1895, 1271, 1083, 611, 531 | 164.610 | 11.398 | 10.660 |
| HOCOO | 3776, 1617, 1374, 1204, 1027, 757, 554, 507, 462 | 13.801 | 11.180 | 6.177 |
| min(cis, cis) | 3807, 1900, 1416, 1203, 982, 771, 767, 634, 516, 436, 251, 134 | 11.565 | 2.678 | 2.174 |
| min(cis, trans) | 3799, 1888, 1428, 1211, 951, 762, 735, 589, 563, 450, 261, 109 | 11.301 | 2.715 | 2.189 |
| min(trans, cis) | 3798, 1950, 1365, 1192, 957, 776, 755, 642, 472, 437, 242, 135 | 11.200 | 2.682 | 2.164 |
| min(trans,trans) | 3771, 1929, 1384, 1196, 895, 743, 711, 600, 462, 440, 278, 104 | 11.098 | 2.708 | 2.177 |
| **$TS_{ISO}$** | 3835, 1908, 1268, 1190, 971, 756, 695, 647, 435, 248, 167, 498*i* | 11.298 | 2.650 | 2.161 |
| **$TS_{HOCl}$** | 2225, 2011, 1273, 1254, 832, 751, 679, 558, 402, 143, 121, 1664*i* | 8.683 | 2.549 | 2.114 |
| **$TS_{HCl}$** | 1929, 1508, 1270, 1057, 827, 797, 724, 512, 410, 232, 177, 852*i* | 10.736 | 2.504 | 2.030 |
| **$TS_{HClO}$** | 2260, 1572, 1228, 993, 854, 653, 559, 357, 190, 116, 80, 1600*i*[c] | 8.211 | 2.312 | 2.043[d] |
| **$TS_{3BD}$** | 3727, 2111, 1251, 965, 669, 615, 447, 287, 415i | 14.066 | 9.205 | 5.643 |

[a] Calculated at the CCSD(T)/cc-pVDZ level of theory. [b] Calculated at the CCSD(T)/cc-pVTZ level of theory. [c] Calculated at the CCSD/6-31G(d) level of theory. [d] Calculated at the CCSD/6-31G(2d,2p) level of theory.

**TABLE 4: CCSD(T) Energies (in au) and Zero-Point Energies (ZPE, in kcal/mol) for the Species involved in the ClO + HOCO Reaction**

| | CCSD(T) energies | | | |
|---|---|---|---|---|
| reactants and products | cc-pVDZ | cc-pVTZ | cc-pVQZ[a] | ZPE[b] |
| Cl | −459.61222 | −459.67622 | −459.69474 | 0.0 |
| HCl | −460.25463 | −460.33722 | −460.36213 | 4.3 |
| ClO | −534.57566 | −534.73436 | −534.78270 | 1.1 |
| HOCl | −535.22970 | −535.39469 | −535.44450 | 8.1 |
| HClO | −535.11962 | −535.29880 | −535.35432 | 5.8 |
| $CO_2$ | −188.14826 | −188.32722 | −188.38451 | 7.2 |
| $CO_3$ | −263.04838 | −263.30396 | −263.38301 | 8.5 |
| HOCO | −188.65022 | −188.83646 | −188.89477 | 13.2 |
| HOCOO | −263.70861 | −263.96965 | −264.05127 | 16.1 |
| transition states | cc-pVDZ | cc-pVTZ | cc-pVQZ[a] | ZPE[b] |
| $\mathbf{TS_{ISO}}$ | −723.34972 | −723.69688 | −723.80419 | 17.3 |
| $\mathbf{TS_{HOCl}}$ | −723.30357 | −723.64756 | −723.75411 | 14.7 |
| $\mathbf{TS_{HClO}}$ | −723.20334[c] | −723.56394[d] | −723.67724[d] | 12.7 |
| $\mathbf{TS_{HCl}}^{\ddagger}$ | −723.28956 | −723.62652 | −723.73204 | 13.5 |
| $\mathbf{TS_{3BD}}$ | −262.67610 | −263.93680 | −264.01843 | 14.4 |

[a] Single-point energy calculated with the CCSD(T)/cc-pVTZ-optimized geometry. [b] Zero-point energies are calculated with the CCSD(T)/cc-pVDZ method. [c] Single-point energy calculated with the CCSD(T)/6-31G(d)-optimized geometry. [d] Single-point energy calculated with the CCSD(T)/6-311G(2df,2p)-optimized geometry.

**TABLE 5: Relative Energetics (kcal/mol) Including the ZPE Corrections for the ClO + HOCO Reaction (min refers to the minima of HOC(O)OCl)**

| | ClO + HOCO → | | | | | | | | |
|---|---|---|---|---|---|---|---|---|---|
| method | HOC(O)OCl | HOC(O)O + Cl | HOCl + $CO_2$ | HClO + $CO_2$ | $\mathbf{TS_{HClO}}$ | HCl + $CO_3$ | min(trans,cis)→ $\mathbf{TS_{HOCl}}$ | min (cis,cis)→ $\mathbf{TS_{HCl}}$ | HOCOO → $\mathbf{TS_{3BD}}$ |
| CCSD(T)/cc-pVDZ | −82.6 | −55.5 | −94.4 | −27.7 | 12.5 | −49.9 | 32.5 | 42.0 | 18.7 |
| CCSD(T)/cc-pVTZ | −83.8 | −45.2 | −93.8 | −35.9 | 2.7 | −45.7 | 34.9 | 48.2 | 18.9 |
| CCSD(T)/cc-pVQZ | −84.3 | −41.2 | −94.1 | −39.8 | −1.4 | −41.8 | 35.4 | 45.6 | 18.9 |
| expt.[33−36] | | | −91.6 ± 1 | | | | | | |

the four-center (HOCl + $CO_2$) elimination reaction, the five-center elimination reaction is also a late transition state, exhibiting product-like character in the transition state. Although this barrier is located 35 kcal/mol below the asymptote of the ClO + HOCO reactants, it is still higher by 12.6 kcal/mol than the transition state $\mathbf{TS_{HOCl}}$, leading to the HOCl + $CO_2$ products. The result suggests that the HCl + $CO_3$ products should be minor for the ClO + HOCO reaction.

**D. Kinetics for the ClO + HOCO Reaction.** Since the dissociation reaction of HOC(O)OCl into either ClO + HOCO or Cl + HOC(O)O is barrierless, we need their potential energies and projected vibrational frequencies along the reaction paths in order to compute the rate coefficients of the relevant reactions. It is formidable to compute these quantities using the high-level ab initio method CCSD(T) owing to the lack of analytic Hessian matrix calculations. In practice, one often encounters the size-consistent and spin contamination problems with the single-determinant-based CCSD(T) method for this radical−radical reaction at large separation distances. Alternatively, in this work, the energies and frequencies are calculated using a multireference second-order perturbation theory[62] CAS(2,4)RS2 together with the 6-31G(d) basis set. That is, the complete active space (CAS) is formed by two electrons and four molecular orbitals (MO). At the dissociation limits, the two electrons are the unpaired electrons whereas the four MOs are the HOMO (highest occupied MO) and LUMO (lowest unoccupied MO) of two moieties. Results are shown in Figure 5. The reaction coordinate is defined by ($R^e_{OO} - R_{OO}$) for the ClO + HOCO channel or by ($R_{OCl} - R^e_{OCl}$) for Cl + HOC(O)O, where $R_{OO}$ and $R_{OCl}$ are the broken bond lengths and $R^e_{OO}$ and $R^e_{OCl}$ are the equilibrium values of the HOC(O)OCl intermediate. One can see that there is no classical barrier for both dissociation reactions. For both branches, the potential curves can be well fitted by the extended Rydberg function[63]

$$V(R) = D_e\{1 - [1 + a_1\Delta R + a_2\Delta R^2 + a_3\Delta R^3]\exp(-b\Delta R)\},\Delta R = |R - R^e| \quad (11)$$

The obtained parameters are $D_e = 4.27746$, $a_1 = 5.26321$, $a_2 = 1.65645$, $a_3 = 27.66761$, and $b = 4.76006$ for ClO and $D_e = 1.71323$, $a_1 = 2.56761$, $a_2 = -3.37138$, $a_3 = 1.19426$, and $b = 2.36503$ for Cl (in units of eV and Å). In order to improve the accuracy of the variational RRKM calculations, the potential curves along the intrinsic reaction path are scaled according to the CCSD(T)/cc-pVQZ bond dissociation energy. Simply, the corresponding bond energies are replaced with $D_e$(O−O) = 3.8284 eV and $D_e$(O−Cl) = 2.2438 eV. The scaled curves are also shown in the top panel of Figure 5.

The vibrational frequencies along the reaction path are displayed in the bottom panel of Figure 5 from the ClO + HOCO reactants to the Cl + HOC(O)O products. There are three disappearing modes for the unimolecular dissociation of the HOC(O)OCl intermediate into Cl + HOC(O)O, whereas there are four modes for that of HOC(O)OCl to ClO + HOCO. In the variational RRKM calculations, the ClO torsional mode of the four disappearing modes for the ClO + HOCO channel is treated as a free rotor with a moment of inertia of 94.90596 amu.

Figure 6 shows the microcanonical rate coefficients of unimolecular dissociation of HOC(O)OCl and its lifetime as a

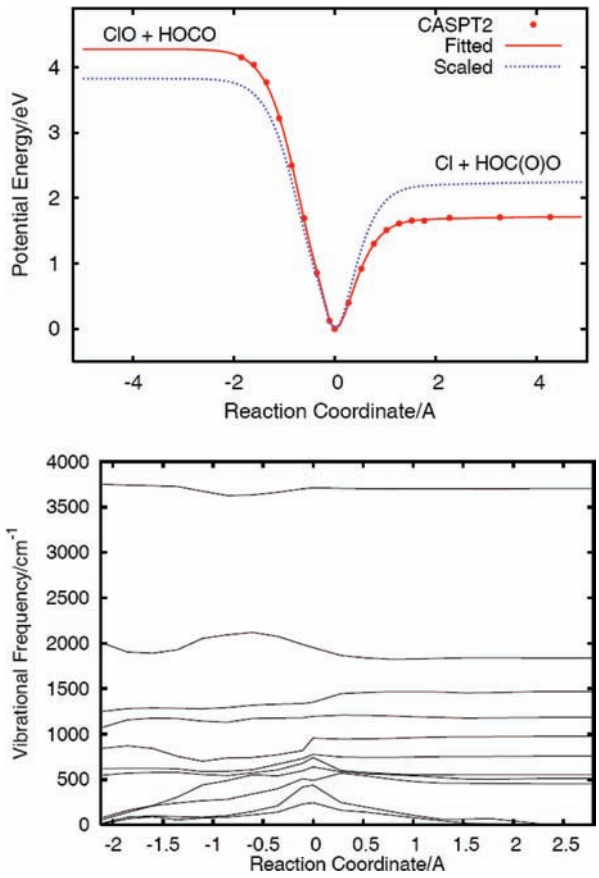


**Figure 5.** Intrinsic reaction path (top) and projected frequencies (bottom) orthogonal to the path for the ClO + HOCO → Cl + HOC(O)O reaction, calculated with the CAS(2,4)RS2/6-31G(d) method. The dashed line in the top panel is the scaled curve according to the CCSD(T)/cc-pVQZ bond energies.

function of collision energy at zero pressure. As the $k_{-1}(E)$ values are very small, they are neglected here. In the RRKM calculations, the number of degenerate reaction paths ($\sigma_p$) is one for the HCl + $CO_3$ product channel, two for HOCl + $CO_2$, and four for Cl + HOC(O)O. Only the (trans,trans) conformer is able to directly access the $\mathbf{TS_{HCl}}$ transition state, whereas both the (cis,trans) and (trans,cis) ones can form the $\mathbf{TS_{HOCl}}$ transition state to dissociate into HOCl + $CO_2$. It clearly shows that the lifetime decreases with energy increasing. The lifetime is about 4.0 ps at low collision energy, while it becomes smaller than 1.0 ps at high energies. The lifetime on the order of picoseconds indicates that the HOC(O)OCl intermediates are only moderate lived complexes at the temperatures of interest.

There are three types of possible products: HOCl + $CO_2$, Cl + HOC(O)O, and HCl + $CO_3$ for the unimolecular dissociation of HOC(O)OCl. As expected, the rate coefficient for the HCl + $CO_3$ products is the smallest owing to the high dissociation barrier discussed above. Interestingly, the products Cl + HOC(O)O are favored over the products HOCl + $CO_2$, although the latter are thermodynamically preferable according to the reaction pathway with the smallest dissociation barrier and the largest exothermicity. This is understandable due to the fact that the bond fission reaction HOC(O)OCl → Cl + HOC(O)O is barrierless. Usually for a barrierless process the corresponding variational transition state is very loose, which can substantially enhance the dissociation flux. As a result, the HOC(O)OCl → Cl + HOC(O)O reaction becomes competitive with the HOC(O)OCl → HOCl + $CO_2$ reaction. The latter is preferable in energy, while the former is dynamically likely.

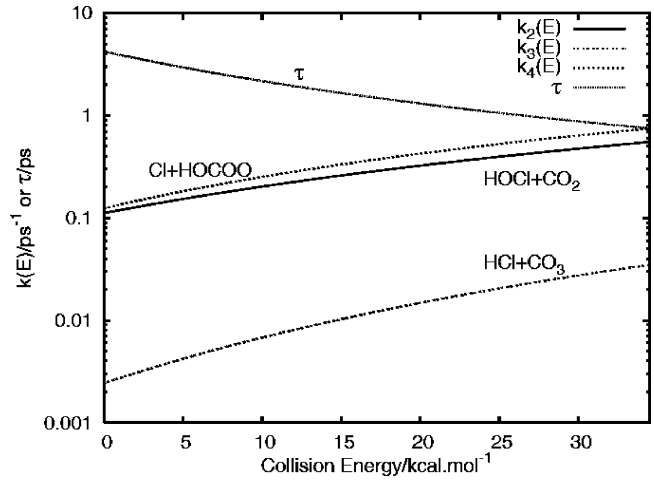


**Figure 6.** Theoretical rate coefficients $k_i(E)$ ($ps^{-1}$) of the unimolecular dissociation of the HOC(O)OCl intermediate and its lifetime $\tau$ (in ps) as a function of the collision energy of the ClO + HOCO reaction. The collision energy is defined as the energy zero at the asymptote of the ClO and HOCO reactants. Please notice the different units in the $y$ axis.

Calculated thermal rate coefficients are given in Table 6. For the ClO + HOCO → HClO + $CO_2$ reaction, the classical barrier height of $\mathbf{TS_{HClO}}$ is taken as 4.3 kcal/mol (after including the zero-point energy corrections, the vibrationally adiabatic ground-state barrier height is reduced to $V_a^G = 2.7$ kcal/mol) calculated with the CCSD(T)/cc-pVTZ//CCSD(T)/6-311G(2df,2p) method. If the CCSD(T)/cc-pVQZ//CCSD(T)/6-311G(2df,2p) energy is used, this $V_a^G$ value is obtained as −1.5 kcal/mol. We believe that the CCSD(T)/cc-pVQZ method has overcorrected the correlation energy since the optimized geometry at CCSD(T)/6-311G(2df,2p) is not very close to that at CCSD(T)/cc-pVQZ owing to the different type of basis sets. In addition, one disappearing mode is treated as a free rotor with a moment of inertia of 167.7904 amu calculated from the structure of the $\mathbf{TS_{HClO}}$ transition state in the RRKM calculations. Results show that the ClO + HOCO reaction is fast. The reaction yields four types of products: Cl + HOC(O)O, HOCl + $CO_2$, HCl + $CO_3$, and HClO + $CO_2$. The product branching ratios for both HCl and HClO product channels are very small. The two major product channels (Cl and HOCl) are nearly equally produced. The overall rate coefficients are negatively temperature dependent at low temperatures, which is consistent with the potential-energy surface of the system. At room temperature, the rate coefficient is predicted to be $4.26 \times 10^{-12}$ $cm^3$ $molecules^{-1}$ $s^{-1}$, with the product branching fractions of Cl (0.518), HOCl (0.469), HCl (0.01), and HClO (0.003). As the uncertainty in the barrier height is about 1.0 kcal/mol, we did a sensitivity test by lowering the $\mathbf{TS_{HOCl}}$ barrier by 1.0 kcal/mol. It was found that the overall rate constants are hardly affected. However, the product branching fractions would be Cl (0.487), HOCl (0.503), HCl (0.01), and HClO (0.003) at room temperature. Therefore, the errors in the product branching ratios should be within 7%.

The ClO + HOCO → HClO + $CO_2$ reaction resembles the ClO + $HO_2$ → HOCl + $O_2$ reaction for the ClO conversion. The latter has a thermal rate coefficient from $4.5 \times 10^{-12}$ to $7.1 \times 10^{-12}$ $cm^3$ $molecules^{-1}$ $s^{-1}$ at room temperature.[64] It is the best known radical−radical reaction[65] that converts ClO to HOCl in atmospheric chemistry. Furthermore, the ClO + HOCO reaction could also play the role of the ClO + OH → Cl + $HO_2$ reaction for the conversion of ClO to Cl. Nevertheless, the ClO + OH reaction is about three times faster than ClO + HOCO. The thermal rate coefficient[66,67] (298 K) of the ClO +

**TABLE 6: Calculated Thermal Rate Coefficients (in $cm^3$ $molecules^{-1}$ $s^{-1}$) for the ClO + HOCO Reaction at Zero Pressure**

| T/K | $10^{12} \times k_{+1}(T)$ | $10^{12} \times k_2(T)$ | $10^{14} \times k_3(T)$ | $10^{12} \times k_4(T)$ | $10^{13} \times k_5(T)$ | $10^{12} \times k_{Tot}(T)$ |
|---|---|---|---|---|---|---|
| 200 | 9.01 | 4.28 | 8.71 | 4.65 | 0.05 | 9.01 |
| 250 | 5.54 | 2.62 | 5.47 | 2.87 | 0.08 | 5.55 |
| 298 | 4.25 | 2.00 | 4.29 | 2.21 | 0.12 | 4.26 |
| 350 | 3.60 | 1.69 | 3.72 | 1.88 | 0.18 | 3.62 |
| 400 | 3.30 | 1.53 | 3.49 | 1.73 | 0.26 | 3.33 |
| 500 | 3.08 | 1.42 | 3.45 | 1.63 | 0.46 | 3.13 |
| 800 | 3.49 | 1.57 | 4.62 | 1.88 | 1.54 | 3.64 |
| 1000 | 3.78 | 1.67 | 5.47 | 2.06 | 2.68 | 4.05 |

OH reaction was measured to be from $1.5 \times 10^{-11}$ to $2.5 \times 10^{-11}$ $cm^3$ $molecules^{-1}$ $s^{-1}$.

In addition, we also estimated the pressure dependence of the reaction using the one-dimensional RRKM/Master equation method[68]

$$\frac{d\mathbf{X}(t)}{dt} = \mathbf{B}\mathbf{X}(t) + \mathbf{C}A(t)B(t) \tag{12}$$

with

$$\mathbf{B} = \varpi(T,P)[\mathbf{P} - \mathbf{I}] - \mathbf{K} \tag{13}$$

and the diagonal matrix **K** has the diagonal elements

$$\mathrm{diag}(\mathbf{K}) = \sum_{p} [k_p(E_1), k_p(E_2), ..., k_p(E_N)] \tag{14}$$

where $A(t)$ and $B(t)$ are the concentrations of the reactants ClO and HOCO as a function of time. $\mathbf{X}(t) = [X(E_1), X(E_2),..., X(E_N)]^T$ is a column vector whose elements are the concentration of the HOC(O)OCl intermediate complex at discrete energies $E_i$ at time $t$. **I** is the identity matrix, whereas **P** is a transition probability matrix. Here, we used an exponential down model.[64] The $j \rightarrow i$ transition probability is then defined as

$$P_{ij} = \frac{1}{N_j} e^{-\gamma(E_j - E_i)}, \text{ if } E_j \geq E_i$$

and

$$= \frac{1}{N_i}\frac{\rho(E_i)}{\rho(E_j)} e^{-(\gamma + 1/k_B T)(E_i - E_j)}, \text{ otherwise} \tag{15}$$

$N_i$ is a normalization factor obtained by detailed balancing principles and $\sum_j P_{ji} = 1$ conditions with the parameter $\gamma = 1/\langle \Delta E_{down} \rangle$. $\rho(E)$ is the density of states of the intermediate. Since the four isomers of HOC(O)OCl are well separated at low energies, a smooth switching function has been employed to calculate the rovibrational density of states as

$$\rho'(E) = \frac{2\rho_\Sigma(E)}{5 - 3\tanh[-4(E - E_{min})/E_b^{iso}]} \tag{16}$$

where $E_{min}$ refers to the energy of the ground state of the global minimum of HOC(O)OCl and $E_b^{iso} = 6.6$ kcal/mol is the isomerization barrier height of isomers. $E_{min}$ has the same energy zero as $E$. In eq 12 **C** is a column vector with the elements

$$\mathbf{C}^T = K_{eq}[k_{-1}(E_1)f(E_1), k_{-1}(E_2)f(E_2), ..., k_{-1}(E_N)f(E_N)] \tag{17}$$

where $K_{eq}(T)$ is the equilibrium constant for the ClO + HOCO $\leftrightarrow$ HOC(O)OCl reaction and $f(E)$ is the normalized Boltzmann−Maxwell distribution of HOC(O)OCl.[68]

The third collision partner is assumed to be $N_2$. The deactivated rate coefficient is given by[65,66]

$$\omega(T,P) = \beta_c Z_{LJ}[N_2] \tag{18}$$

where $\beta_c$ and $Z_{LJ}$ are the collision efficiency and the Lennard−Jones (LJ) collision frequency, respectively. They are determined by Troe's method[69,70] using an exponential down energy of $\langle \Delta E_{down} \rangle = 157$ $cm^{-1}$, taken from the value of the $N_2$−HOCO system,[71] and the LJ parameters: $d = 3.61$ Å and $\varepsilon_{N_2-HOC(O)OCl} = 509$ $cm^{-1}$. These parameters are calculated with the MP2/6-31G(d,p) method. The $\varepsilon_{N_2-HOC(O)OCl}$ value was determined by the global minimum potential well for the $N_2$ and HOC(O)OCl interactions. The hard-sphere radius $d$ was estimated by the center-of-mass distance between these two partially optimized moieties at which the potential energy of the complex is zero relative to the $N_2$ + HOC(O)OCl dissociation limit. However, the dynamics average has not been carried out for these LJ parameters. This may introduce errors by 10% to underestimate $d$ or to overestimate $\varepsilon_{N_2-HOC(O)OCl}$. At room temperature, therefore, such errors could introduce uncertainty into the deactivated rate coefficient in eq 16 by up to 11.3%.

Calculated rate coefficients are displayed in Figure 7, together with the rate coefficient for the stabilization of intermediates. In the calculations, the energy grid size was taken as 25 $cm^{-1}$ with a total of 1680 ($N$) grids, which gives an energy span of 120.0 kcal/mol. The results show that the pressure dependence of the product branching ratios for the ClO + HOCO reaction

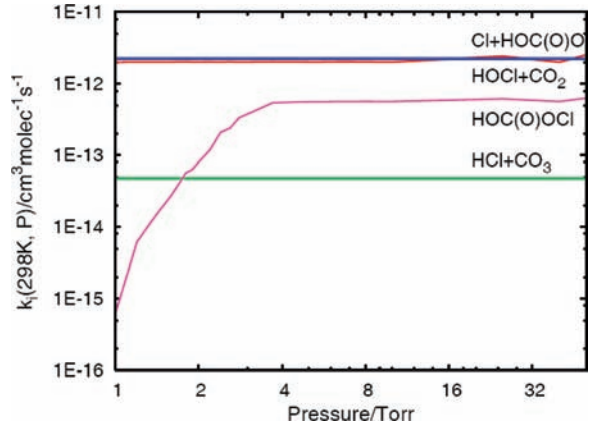


**Figure 7.** Thermal rate coefficients of the ClO + HOCO reaction to either Cl + HOCOO, HOCl + $CO_2$, HCl + $CO_3$, or the HOC(O)OCl complex as a function of pressure.

(except for stabilization of HOC(O)OCl) is rather weak. This is because the exit barriers are much lower than the reactant asymptote, and the intermediates are only moderate lived during the reaction course. The only competitive channel is HCl + $CO_3$ owing to its high dissociation barrier. At the high-pressure limit, the recombination rate coefficient[68] of the forward ClO + HOCO reaction is obtained as $k_{rec} = 5.32 \times 10^{-12}$ cm$^3$ molecules$^{-1}$ s$^{-1}$ while the unimolecular rate constant of its backward reaction is $k_{uni} = 1.68 \times 10^{-12}$ ps$^{-1}$. The real bimolecular rate coefficients (in cm$^3$ molecules$^{-1}$ s$^{-1}$) are calculated to be $2.17 \times 10^{-12}$ for HOCl, $2.26 \times 10^{-12}$ for Cl, $4.84 \times 10^{-14}$ for HCl, and $6.20 \times 10^{-13}$ for the formation of HOC(O)OCl complex. By including the pressure-independent rate constant for the HClO + $CO_2$ products, the overall bimolecular rate coefficient is predicted to be $k_{Tot}(298\ K) = 5.22 \times 10^{-12}$ cm$^3$ molecules$^{-1}$ s$^{-1}$ at the high-pressure limit.

## IV. Summary

CCSD(T) methods have been employed to study the ClO + HOCO reaction by computing the stationary points on the singlet ground-state potential-energy surface of the system. The minimum energy paths show that the ClO + HOCO reaction occurs via a direct hydrogen abstraction mechanism and/or an addition mechanism through the HOC(O)OCl intermediate. The addition mechanism is more energetically preferred. On the basis of the high-level ab initio calculations, the thermal rate coefficients and the product branching ratios have been evaluated using the variational RRKM approach. The kinetics results show that the ClO + HOCO reaction yields an array of products such as Cl + HOC(O)O, HOCl + $CO_2$, HCl + $CO_3$, and HClO + $CO_2$. However, only the Cl and HOCl channels are predicted to be major. The dynamically favored Cl + HOC(O)O products result from the loose variational transition state along the Cl−O bond cleavage path of HOC(O)OCl.

The thermal rate coefficients of the ClO + HOCO reaction are negatively dependent on temperature at low temperatures. At room temperature, the thermal rate coefficient is determined to be $4.26 \times 10^{-12}$ cm$^3$ molecules$^{-1}$ s$^{-1}$, with a near unity product branching ratio of Cl to HOCl. These results also suggest that the ClO + HOCO reaction could play the same functions as the ClO + $HO_x$ reactions for the depletion of ozone and conversion of CO into $CO_2$. However, the role of the ClO + HOCO reaction should be minor due to the low concentration of HOCO.

**Acknowledgment.** This work was performed at Brookhaven National Laboratory under contract no. DE-AC02-98CH10886 with the U.S. Department of Energy and supported by its Division of Chemical Sciences, Office of Basic Energy Sciences.

**Supporting Information Available:** Table 1 contains the CCSD(T) equilibrium geometries for the species involved in the ClO + HOCO reaction. This material is available free of charge via the Internet at http://pubs.acs.org.

## References and Notes

(1) Eston, R. E. *Chem. Rev.* **1995**, *99*, 2115.
(2) Ravishankara, A. R.; Thompson, R. L. *Chem. Phys. Lett.* **1983**, *99*, 377.
(3) Jonah, C. D.; Mulac, W. A.; Zeglinski, P. *J. Phys. Chem.* **1984**, *88*, 4100.
(4) Forster, R.; Frost, M.; Fulle, D.; Harmann, H. F.; Hippler, H.; Schlepegrell, A.; Troe, J. *J. Chem. Phys.* **1995**, *103*, 2949.
(5) Frost, M. J.; Sharkeley, P.; Smith, I. W. M. *J. Phys. Chem.* **1993**, *89*, 12254.
(6) Alagia, M.; Bulucani, N.; Casavecchia, P.; Stranges, D.; Volpi, G. G. *J. Chem. Phys.* **1993**, *98*, 8341.
(7) DeMore, W. B. *Int. J. Chem. Kinet.* **1984**, *16*, 1187.
(8) Paragkeopoulous, G.; Irwin, R. S. *J. Chem. Phys.* **1984**, *80*, 259.
(9) Hufzumahaus, A.; Stuhl, F. *Ber. Bunsen Ges. Phys. Chem.* **1984**, *88*, 557.
(10) McCabe, D. C.; Gierczak, T.; Talukdar, R. K.; Ravishankara, A. R. *Geophys. Res. Lett.* **2001**, *28*, 3135.
(11) Yu, H.-G.; Muckerman, J. T.; Sears, T. J. *Chem. Phys. Lett.* **2001**, *349*, 547.
(12) Duncan, T. V.; Miller, C. E. *J. Chem. Phys.* **2000**, *113*, 5138.
(13) Jacox, M. E. *J. Chem. Phys.* **1988**, *88*, 4598.
(14) Radford, H. E.; Wei, W.; Sears, T. J. *J. Chem. Phys.* **1992**, *97*, 3989.
(15) Sears, T. J.; Farvzy, M. W.; Johnson, P. M. *J. Chem. Phys.* **1992**, *97*, 3996.
(16) Petty, T. J.; Moore, C. B. *J. Chem. Phys.* **1993**, *99*, 47.
(17) Miyoshi, A.; Matsui, H.; Washida, N. *J. Chem. Phys.* **1994**, *100*, 3532.
(18) Ruscic, B.; Schwarz, M.; Birkowitz, J. *J. Chem. Phys.* **1989**, *91*, 6780.
(19) Milligan, D. E.; Jacox, M. E. *J. Chem. Phys.* **1971**, *54*, 927.
(20) Petty, J. T.; Harrison, J. A.; Moore, C. B. *J. Chem. Phys.* **1993**, *97*, 11194.
(21) Olkhov, R. V.; Li, Q.; Osborne, M.C.; Smith, I. W. M. *Phys. Chem. Chem. Phys.* **2001**, *3*, 4522.
(22) Yu, H.-G.; Muckerman, J. T. *J. Phys. Chem. A* **2006**, *111*, 5312.
(23) Li, Q.; Osborne, M. C.; Smith, I. W. M. *Int. J. Chem. Kinet.* **2000**, *32*, 85.
(24) Yu, H.-G.; Francisco, J. S.; Muckerman, J. T. *J. Chem. Phys.* **2008**, *129*, 064301.
(25) Yu, H.-G.; Muckerman, J. T.; Francisco, J. S. *J. Chem. Phys.* **2008**, *128*, 244315.
(26) Yu, H.-G.; Muckerman, J. T.; Francisco, J. S. *J. Chem. Phys.* **2007**, *127*, 094302.
(27) Yu, H.-G.; Muckerman, J. T.; Francisco, J. S. *J. Phys. Chem. A* **2005**, *109*, 5230.
(28) Yu, H.-G.; Poggi, G.; Francisco, J. S.; Muckerman, J. T. *J. Chem. Phys.* **2008**, *129*, 214307.
(29) Yu, H.-G.; Francisco, J. S. *J. Phys. Chem. A* **2009**, *113*, 3844.
(30) Poggi, G.; Francisco, J. S. *J. Chem. Phys.* **2004**, *120*, 5073.
(31) Francisco, J. S.; Muckerman, J. T. Yu, H.-G. *Acc. Chem. Res.*, submitted for publication.
(32) Lary, D. J.; Chipperfield, M. P.; Toumi, R. *J. Atmos. Chem.* **1995**, *21*, 61.
(33) Reimann, B.; Kaufman, F. *J. Chem. Phys.* **1978**, *69*, 2925.
(34) Stimpfle, R. M.; Perry, R. A.; Howard, C. T. *J. Chem. Phys.* **1979**, *71*, 5183.
(35) Leu, M. T. *Geophys. Res. Lett.* **1980**, *7*, 173.
(36) Leck, J. T.; Cook, J. E. L.; Birks, J. W. *J. Chem. Phys.* **1980**, *72*, 2364.
(37) Knight, G. P.; Beiderhase, T.; Helleis, F.; Moortgat, G. K.; Crowley, J. N. *J. Phys. Chem. A* **2000**, *104*, 1674.
(38) Hickson, K. M.; Keyser, L. F.; Sander, S. P. *J. Phys. Chem. A* **2007**, *111*, 8126.
(39) Finkbeiner, M.; Crowley, J. N.; Horie, O.; Muller, R.; Moortgat, G. K. *J. Phys. Chem.* **1995**, *99*, 16264.
(40) Xu, Z.F.; Zhu, R. S.; Lin, M. C. *J. Phys. Chem. A* **2003**, *107*, 3841.
(41) Pople, J. A.; Head-Gordon, M.; Raghavachari, K. *J. Chem. Phys.* **1987**, *87*, 5968.
(42) Dunning, T.H., Jr. *J. Chem. Phys.* **1989**, *93*, 1007.
(43) Kendell, R. A.; Dunning, T.H., Jr.; Harrison, R. J. *J. Chem. Phys.* **1992**, *96*, 6796.
(44) Schlegel, H. B. *J. Comput. Chem.* **1982**, *3*, 214.
(45) Raghavachari, K.; Twiks, G. W.; Pople, J. A.; Head-Gordon, M. *Chem. Phys. Lett.* **1989**, *157*, 479.
(46) Watts, J. D.; Gauss, J.; Bartlett, R. J. *J. Chem. Phys.* **1993**, *98*, 8718.
(47) Garrett, B. C.; Truhlar, D. G. *J. Phys. Chem.* **1979**, *83*, 2921.
(48) Liu, Y.-P.; Lu, D.-H.; Gonzalez-Lafont, A.; Truhlar, D. G.; Garrett, B. C. *J. Am. Chem. Soc.* **1993**, *115*, 7806.
(49) Fernandez-Ramos, A.; Miller, J. A.; Klippenstein, S. J.; Truhlar, D. G. *Chem. Rev.* **2006**, *106*, 4518.
(50) Miller, W. H. *J. Am. Chem. Soc.* **1979**, *101*, 6810.
(51) Truhlar, D. G.; Gordon, M. S. *Science* **1990**, *249*, 491.
(52) Hase, W. L. *Acc. Chem. Res.* **1983**, *16*, 258.
(53) Baer, T.; Hase, W. L. *Unimolecular Reaction Dynamics: Theory and Experiments*; Oxford University Press: New York 1996.
(54) Beyer, T.; Swinehart, D. R. *ACM Commun.* **1973**, *16*, 379.
(55) Frisch, M. J.; Trucks, G. W., Schlegel, H. B.; et al. *Gaussian 03*, Revision B.04; Gaussian, Inc.L Pittsburgh, PA, 2003.

(56) MOLPRO (version 2006 1) is an ab initio program for molecular electronic structure calculations, written by H.-J. Wener and P. J. Knowles, and containing contributions from a number of other authors.

(57) Electronic Supplementary Information: The CCSD(T) equilibrium geometries for the species involved in the ClO + HOCO reaction, where units are Angstroms for length and degress for angles.

(58) Barnes, R. J.; Sinha, A. *J. Chem. Phys.* **1997**, *107*, 3730.

(59) Chase, W. W., Jr.; Davies, C.A.; Downey, R., Jr.; Frurip, D. J.; McDonald, R. A.; Syvervnd, A. N. *J. Phys. Chem. Ref. Data, Suppl.* **1985**, *1*, 14.

(60) Feller, D.; Dixon, D. A.; Francisco, J. S. *J. Phys. Chem. A* **2003**, *107*, 1604.

(61) Matus, M. H.; Nguyen, M. T.; Dixon, D.A.; Petersen, K. A.; Francisco, J. S. *J. Phys. Chem. A* **2008**, *112*, 9623. Chase, M.W., Jr.; et al. *J. Phys. Chem. Ref. Data Monogr.* **1998**, *9*, 1–1951.

(62) Werner, H.-J. *Mol. Phys.* **1996**, *89*, 645.

(63) Murrell, J. N.; Carter, S.; Farantos, S. C.; Huxley, P.; Varandas, A. J. C. *Molecular Potential Energy Functions*; Wiley: Chichester, 1984.

(64) Hickson, K. M.; Keyser, L. F.; Sander, S. P. *J. Phys. Chem. A* **2007**, *111*, 8126.

(65) Lary, D. J.; Chipperfield, M. P.; Toumi, R. *J. Atmos. Chem.* **1995**, *21*, 61.

(66) Ravishankara, A. R.; Eisele, F. L.; Wine, P. H. *J. Chem. Phys.* **1983**, *78*, 1140.

(67) Burrows, J. P.; Wallington, T. J.; Wayne, R. P. *J. Chem. Soc., Faraday Trans. II* **1984**, *80*, 957.

(68) Gilbert, R. G.; Smith, S. C. *Theory of Unimolecular and Recombination Reactions*; Blackwell Scientific Publications: Oxford, 1990.

(69) Troe, J. *J. Chem. Phys.* **1977**, *66*, 4758.

(70) Troe, J. *J. Phys. Chem.* **1979**, *83*, 114.

(71) Joshi, A. V.; Wang, H. *Int. J. Chem. Kinet.* **2006**, *38*, 57.

JP9040088